Determining spinal length and thoracic volume in adolescent idiopathic scoliosis during growth using BoneMRI

R.E. Buijs, D.M Cornelissen, D. Devetzis, D. Le, J. Zhang

Utrecht University & University of Technology Eindhoven

I. INTRODUCTION

Scoliosis is a three-dimensional spinal deformation. Adolescent Idiopathic Scoliosis (AIS) accounts for 90% of idiopathic scoliosis cases [1]. Curve severity is measured by the Cobb angle and is often seen in combination with vertebral rotation [1]. During growth, scoliosis progresses, which can lead to back pain and in severe cases (Cobb angle > 40 degrees) to rib cage deformities and eventually restrictive or obstructive pulmonary disease [2].

Mild to severe AIS is treated with a brace or spinal surgery, depending on spinal length and thoracic volume during growth. Bracing before the peak height velocity has been shown to prevent curves from reaching the surgical threshold (a Cobb angle of at least 40 degrees) [3]. In contrast, after skeletal maturation has been reached, surgery is the preferred treatment since the deformities cannot be corrected during the bone growth phase anymore. To prevent patients from having to undergo multiple spinal surgeries due to further progression of the scoliotic curve, surgery is usually not performed during the growth phase.

Currently, spinal growth and thoracic volume is assessed using anteroposterior radiographs and measuring sitting height over time. Thoracic volume is chosen over trunk volume due to its more consistent definition, is less sensitive to variations in fat distribution and food intake. Furthermore, thoracic volume provides insight into pulmonary function.

A more accurate representation of these parameters can be derived from a three-dimensional imaging technique. BoneMRI allows ionizing radiation free three-dimensional imaging, while allowing visualization of both soft tissues and the vertebrae, including their cortex [4]. This imaging technique is deep learning trained using computed tomography scans as a comparator. Therefore, BoneMRI produces artificial Hounsfield Units, allowing comparison between multiple centers and CT. Furthermore, the deep learning algorithm used for BoneMRI is fit for adolescent spines [5].

The aim of the proposed research is to evaluate spinal length and thoracic volume in adolescents acquired from BoneMRI images as parameters to quantify scoliosis severity. To derive spinal length and thoracic time-efficiently from BoneMRI images, segmentation or deep learning should be used to determine and track spinal length and thoracic volume. We present a method for automatically segmenting individual vertebrae, ribs, and the sternum which can be used to calculate these parameters. Segmenting individual vertebrae allows location specific measurement of every associated parameter. These parameters will then be compared between a healthy group of participants and a group of AIS patients, to determine the accuracy of this method.

II. METHODS

A. Image acquisition

1) Participants

The participants for this research should be between the ages of 10 and 18 years old. The participant pool should consist of two approximately equal groups of which one consists of healthy participants, and the other of participants diagnosed with Adolescent Idiopathic Scoliosis (AIS).

2) Image acquisition protocol

In this research, the relatively novel method called BoneMRI will be used to obtain three-dimensional, CT-like images of the spine and the trunk (BoneMRI, MRIguidance B.V.).

The acquisition protocol is based on the protocol used by Staartjes et al. [4]. All MRI images will be acquired in supine position using a 1.5 T scanner with a body coil. All patients should be positioned with the T1 to the L5 within the specified FOV. A spoiled T1-weighted multiple gradient echo sequence with two echoes (TR = 7 ms, TE1 = 2.1 ms, TE2 = 4.2 ms, FOV = 500 x 250 x 90 mm, voxel size = 0.74 x 0.74 x 0.9 mm) will be obtained for BoneMRI reconstruction. Similar to Staartjes et al., we will use a high-frequency encode bandwidth to minimize geometrical distortions (BW > 500 Hz/pix).

As the participants of this research are between 10 and 18 years old and might experience anxiety related to the MRI scanner, this method does not use breath-holding but opts for free-breathing MRI. To minimize breathing-related motion artifacts, we will apply respiratory gating during the acquisition of the MR images using a bellows, as described by Janos et al. [6].

3) Synthetic CT reconstruction

Using a patch-based convolutional neural network (a 3D extension of the U-net), synthetic computed tomography images will be generated from the images acquired by the

BoneMRI protocol [4]. This deep learning model will be trained using paired MRI and CT data and is based on a model used by other BoneMRI studies [4], [7].

B. Deep learning for segmentation of skeletal structures

The process of analyzing the images and calculating spinal length and thoracic volume from the images, the data first needs to be preprocessed. The next step is creating a mask of skeletal structures including the vertebrae, ribs and sternum and performing data augmentation to enable segmentation of the regions of interest using deep learning. In this study, we will consider the spinal length as the length of the spine from the T1 to L5 vertebrae and we will define the thoracic volume as the rib cage volume from the jugular notch to the tenth rib. The following paragraphs contain a more elaborate description of these processes.

1) Data preprocessing

Data preprocessing is one of the essential steps before training a deep-learning model. In general, to facilitate model training, normalization of the data is performed, to ensure the domain of input data is within similar range. However, the acquired synthetic CT data are expressed in Hounsfield Units, which are absolute intensity values. Although not directly measured, it is a measure based on a linear transformation of the baseline linear attenuation coefficient, where distilled water is defined to be zero Hounsfield Units [8]. For this reason, we are opting out of normalization of the absolute intensities, to conserve underlying information on bone density.

Other preprocessing steps such as reduction or removal of noise, extracting useful features and removing useless features may improve the performance of the model [9]. For example, to remove outliers, a histogram of all intensity values is made and a range is chosen in the histogram in such a way that the outliers are left out of this range.

2) Labeling

Ground truth data needs to be available to train a supervised machine learning model. These ground truth data can be created by labeling the images. For all images that are available, a copy will be made in which the pixels of each vertebrae will be one-hot encoded from 1 to 17 and the ribs from the first to the tenth as well as the sternum will be labeled as 18, where the pixels in T1 get 1, T2 get 2, …, L5 get 17. Everything that is not part of skeleton structures we considered gets label 0.

The labeling process is best done by a medical expert with knowledge of scoliosis. This ensures that the spine is better segmented than in the case someone without knowledge about the anatomy of scoliosis patients will do the segmentation.

3) Data augmentation

Deep-learning models require a substantial amount of data to converge. High costs, privacy concerns and the prevalence of AIS are examples which play a role in the availability of data. Data augmentation, however, can be used to increase the size of the dataset. The goal of data augmentation is to generate additional data that can be used for training the deep-learning model, making the model more robust [6]. The general process to perform data augmentation is to apply geometric transformations to the existing data and add the transformed data to the dataset. Examples of transformation operations to consider are scaling, translating, rotating, and shearing the data. However, since the model will be used on images that are generally in the same orientation, the parameters of these transformation (e.g., angle, scaling factor, etc.) are constraint within a range, such that the range of transformation is within the domain of AIS. It is also possible to change the value of certain pixels/voxels of the data. Examples of this are gamma correction and linear contrast. Noise injection is a technique where noisy data is simulated. Noise injection can be done with different types of noise, such as gaussian noise, uniform noise or salt and pepper noise [10].

4) Data splitting

The last step of the preprocessing process is to split the data into a training set, test set, and a validation set. For evaluating the architecture that is used we will use K-fold cross validation (KCV). KCV splits the dataset in k groups of size *total data/k* where one of these groups is used as the test set and is taken out of the training process. After training, the model is evaluated on this test set. This procedure is then repeated until every group has been the test set. For every time a new set is chosen as test set, a different model can be used. Finally, all the results can be compared with each other and the model with the best performance is selected.

5) Model architecture

The choice of deep-learning architecture for vertebrae segmentation depends on several factors. Convolutional Neural Networks (CNN) may be our preferred choice due to inductive biases and assumptions we have on the image data, such as the presence of specific patterns or structures. Traditional CNNs such as the U-Net [11], have been widely used the past decades for semantic segmentation tasks, particularly in the field of medical imaging. However, the traditional U-Net is designed for 2D segmentation and would have to be extended to 3D volumetric semantic segmentation, using for example 3D convolution layers and 3D max-pooling. Additionally, the last layer of the model should be a Softmax layer.

The segmentation model should output a predicted segmentation mask of which its dimensions equal the input image dimensions. In an N-class segmentation task, the output should be N number of channels for each voxel where each channel depicts the probability of the voxel belonging to a certain class and thus vertebra. To train such a model, a loss function must be defined. A commonly used loss function for semantic segmentation is the voxel-wise cross entropy loss. The final output is then a segmentation mask where each voxel value corresponds to a vertebra, ranging from T1 to L5, or the composite structure of ribs and the sternum.

6) Objective metrics

To quantitatively assess the performance of the model, several commonly used objective metrics can be of interest. The Dice Similarity Coefficient (DSC) can be used to measure the overlap between the predicted mask and ground truth segmentation mask. As this is a multiclass segmentation, the DSC score is computed for every class. Additionally, the DSC

metric is easily interpretable and is well-suited for tasks such as segmentation.

Another objective metric of consideration is the Hausdorff distance, which is defined as the maximum of minimum distances between ground truth and predicted mask.

7) Segmentation results

To show the segmentation results we expect to get, we use the dataset from Large Scale Vertebrae Segmentation Challenge (VerSe) and use it to generate all the figures in our proposal [12]–[14]. The segmentation mask includes all the vertebra within the CT images and each of them has its own label (corresponding to different color in theask). Since the dataset doesn't have the mask for ribs and sternum, we choose one image which includes the vertebra from C7 to L6 and segment the sternum and ribs from 1st to 10th manually on the 3D Slicer software. Finally, we show the 3D segmentation results on the software and screenshot for the anteroposterior and lateral view (Fig 1).

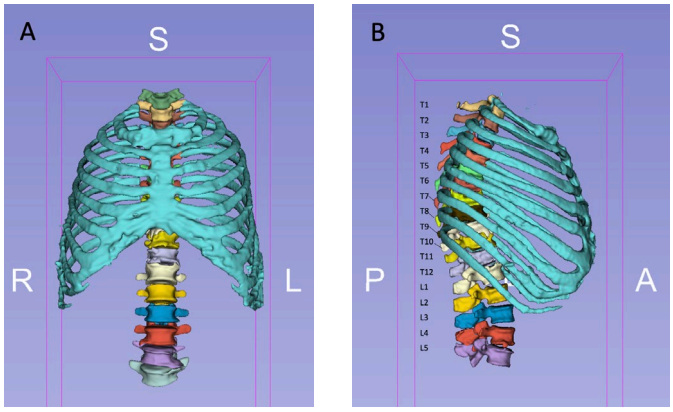

Fig. 1. (A) The anteroposterior view of segmented skeletal structures (B) The lateral view of segmented skeletal structures. Adapted from [12].

C. Spinal length calculation

Most manual spinal length is currently measured by calculating the distance between intervertebral disks or endplates. The spinous and transverse processes are generally not used [15]. Mimicking this, the centroid of each segmented vertebral body from T1 up until L5 will be calculated. Through
the centroids, a 3D vertebral body line will be calculated using a polynomial function. A healthy upright spine from T1-L5 exhibits only three flexion points, all in the sagittal plane. These points correspond to are the maximum thoracic kyphosis, maximum lumbar lordosis, and the transition from kyphosis to lordosis. To fit a polynomial through these points, a least a fourth-degree curve is required. In AIS, there is also a coronal imbalance, originating from a primary and sometimes a secondary curve. Therefore, up to 6 additional flexion points can be assigned: both maximum curve apexes and two sets of upper and lower end vertebrae. This means a seventh-degree curve is used to describe the coronal aspect of the 3D vertebral body line. Due to the usage of centroids and the symmetry of the vertebral bodies, shifts along the longitudinal axis are not influenced by AIS [16]. Using these limitations, the polynomial is calculated. For initialization, a first-degree line is used. Optimalisation is done using least squares fitting (LSF). A lateral view of a similar method is visualized in Fig. 2.
Using the proposed method, the centre of each vertebral body is not always the exact centre, due to the limited spatial resolution of the BoneMRI. This results in a slight over- or underestimation of the spinal length.

Fig. 2. The segmentation mask of vertebra (C7 to L5) overlays the original CT sagittal image. Here, the centroid of T1-L4 is estimated and marked on the image. A curve is fitted to connect all the points. Adapted from [12].

D. Thoracic volume calculation

There are currently several medical image processing software that can calculate thoracic volume by extracting the skeletal structure and then reconstructing the surface thoracic model, such as Mimics [17]. However, they are all semi-automatic and thus require manual annotation and calibration which depend on the clinical experience of operators and extra training. Moreover, only one patient's image data can be analyzed at a time on the software, so large batches of images present a very high workload. As a result, we propose a two-step automatic analysis method: 1) extracting the thoracic skeletal structure by deep learning and 2) calculating the thoracic volume after surface reconstruction. It is important to note that, given the thoracic volume is typically defined as the volume of a transverse section from the jugular notch to the 10th rib, ribs' mask should only encompass the first to the 10th ribs [18].

In order to obtain more accurate calculation results in the next steps, we need to optimize the segmentation model to perform best by adjusting parameters and trying different architectures.

1) Surface reconstruction

After obtaining the skeletal structure, we need to expand it to an enclosed chamber for volume calculation. The upper surface is the axial plane passing through the jugular notch, which is the top of the sternum, and the bottom surface can be estimated as the axial plane through the lowest point of 10th rib. These two surfaces are within the areas enclosed by 1st rib and 10th rib, respectively. The surface enclosed by the ribs, sternum, and spine acts as the sides of the cavity, but since there are gaps

between the ribs, they need to be filled to create a continuous surface. Here we can use simple morphological operation-dilation or other surface reconstruction methods such as the Marching Cubes algorithm.

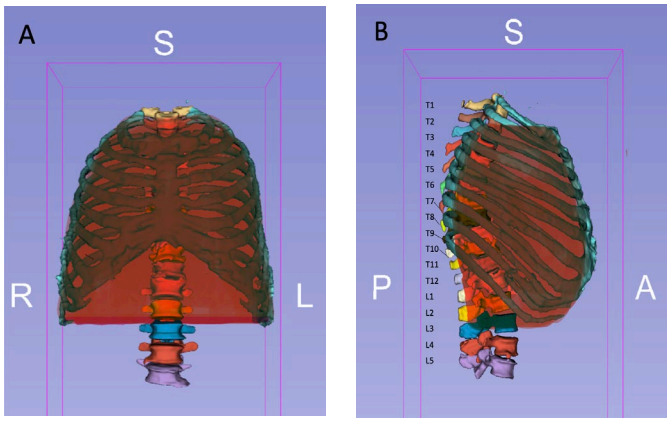

Fig. 3. (A) The anteroposterior projection of reconstructed thoracic volume (B) The lateral projection of reconstructed thoracic volume. Adapted from [12].

2) Volume calculation

Since we already have an empty cavity, the volume enclosed by the inner surface is the thoracic volume which can be measured by simply summing up the total number of voxels multiplied by individual voxel's size. Steps 1 and 2 can be automatically implemented through algorithms, and finally we can obtain the thoracic volumes of a batch of patient's images. The sketch images of our calculation method are shown in Fig 3 and the volume marked in red is our expected volume.

3) Left and right thoracic volumes

Due to abnormal curvature of the spine, not only the total thoracic volume is affected but also the left and right thoracic volumes. The left thoracic volume is typically smaller than the right one, and the former decreased more than the latter in AIS. In that way, the asymmetry between left and right thoracic volume will increase in patients with scoliosis [19]. In addition, the change of left and right thoracic volumes between the preoperative and postoperative scan can reflect the result of scoliosis surgery [20]. Whereas current studies commonly use lung volume to calculate the left and right volume. Since we have calculated the total thoracic volume, it's a good attempt to split the thoracic volume into the left and right part based on the plane enclosed by the sternum and the curved line of the spine.

4) Reference volume

To verify the performance of our proposal, we need to obtain the reference volume for comparison. It can be measured by outlining the inner contour of the ribs per slice (within the range from 1st rib to 10th rib) manually and calculating the area enclosed by it in analysis software such as ITK-SNAP. The final volume is the sum of the area multiplied by the thickness of slices [21]. Fig 4 shows the annotated line and segmented area in one slice. The segmented rib is in green, the annotation line is in yellow, and the grey area is enclosed by the yellow line.

The drawback of this method is that the measured volume is an estimate value, since we use the axial plane through the lowest point of 10th rib as the bottom of the thorax, but it should be the diaphragm in anatomy. Whereas, considering our research subjects are patients with AIS, the thoracic volume we measured is sufficient to reflect thoracic growth which we focus on.

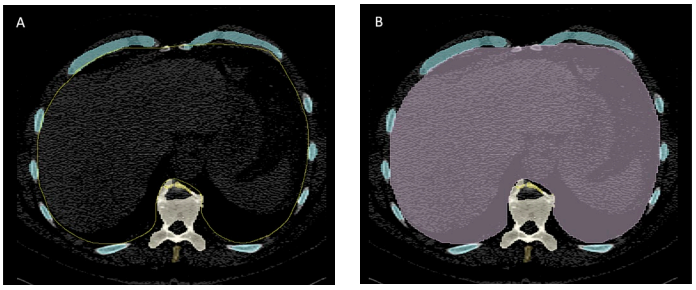

Fig. 4. One of the axial slices in one patient's CT images. (A) shows the annotation line and (B) shows the area considered. Adapted from [12].

III. DISCUSSION

In summary, the proposed research will make use of the novel method called BoneMRI to obtain MRI images of the spine and the thorax and convert these to CT-like scans for assessment of spine length and thoracic volume. After image acquisition and conversion to CT-like data, image analysis is performed with the following steps: *1) data preprocessing*, *2) labeling, 3) data augmentation* and *4) data splitting* to train the spinal segmentation model and *5) vertebrae and thorax segmentation* using a trained CNN U-Net model. After this, the length of the spine can be calculated by fitting a seventh-degree polynomial through the midpoints of the individual vertebrae. The volume of the thorax can be calculated from the volume obtained during the segmentation.

It should be noted that the amount of data needed for training of the segmentation model may be very limited, despite the described augmentation of the available data. As scoliosis is a relatively rare condition with a prevalence of 0.47 to 5.2% of the population and not each patient with AIS might be scanned, the availability of training data can be a limiting factor of the training of the model, thereby affecting the applicability of the proposed method [22]. Furthermore, the performance of the model partially depends on the annotation process and should preferably be performed by medical experts. However, as mentioned before, the reproducibility of the final model is limited by the need for interaction of a professional to manually label the vertebrae, thereby eliminating the involvement of human error.

All in all, this novel method and its limitations should be researched to evaluate the possibilities of routine imaging the spine and trunk of patients with AIS with BoneMRI. Because of its higher accuracy and lower radiation dose compared to current procedures, the proposed method could be a key component in increasing our current knowledge on the development of this condition.

REFERENCES

[1] M. R. Konieczny, H. Senyurt, and R. Krauspe, "Epidemiology of adolescent idiopathic scoliosis," *J Child Orthop*, vol. 7, no. 1, pp. 3–9, Feb. 2013, doi: 10.1007/s11832-012-0457-4.

[2] A. L. Kuznia, A. K. Hernandez, and L. U. Lee, "Adolescent Idiopathic Scoliosis: Common Questions and Answers.," *Am Fam Physician*, vol. 101, no. 1, pp. 19–23, Jan. 2020.

[3] J. P. Y. Cheung, P. W. H. Cheung, D. Samartzis, and K. D.-K. Luk, "Curve Progression in Adolescent Idiopathic Scoliosis Does Not Match Skeletal Growth," *Clin Orthop Relat Res*, vol. 476, no. 2, pp. 429–436, Feb. 2018, doi: 10.1007/s11999.0000000000000027.

[4] V. E. Staartjes, P. R. Seevinck, W. P. Vandertop, M. van Stralen, and M. L. Schröder, "Magnetic resonance imaging–based synthetic computed tomography of the lumbar spine for surgical planning: a clinical proof-of-concept," *Neurosurg Focus*, vol. 50, no. 1, p. E13, Jan. 2021, doi: 10.3171/2020.10.FOCUS20801.

[5] L. R. Chong, K. Lee, and F. Y. Sim, "3D MRI with CT-like bone contrast – An overview of current approaches and practical clinical implementation," *Eur J Radiol*, vol. 143, p. 109915, Oct. 2021, doi: 10.1016/j.ejrad.2021.109915.

[6] S. Janos, G. R. Schooler, J. S. Ngo, and J. T. Davis, "Free-breathing unsedated MRI in children: Justification and techniques," *Journal of Magnetic Resonance Imaging*, vol. 50, no. 2, pp. 365–376, Aug. 2019, doi: 10.1002/jmri.26644.

[7] M. C. Florkow *et al.*, "Deep learning–based MR-to-CT synthesis: The influence of varying gradient echo–based MR images as input channels," *Magn Reson Med*, vol. 83, no. 4, pp. 1429–1441, Apr. 2020, doi: 10.1002/mrm.28008.

[8] T. D. DenOtter and J. Schubert, *Hounsfield Unit*. 2023.

[9] D. Stojnev and A. Stojnev Ilić, "Preprocessing Image Data for Deep Learning," in *Proceedings of the International Scientific Conference - Sinteza 2020*, Beograd, Serbia: Singidunum University, 2020, pp. 312–317. doi: 10.15308/Sinteza-2020-312-317.

[10] P. Chlap, H. Min, N. Vandenberg, J. Dowling, L. Holloway, and A. Haworth, "A review of medical image data augmentation techniques for deep learning applications," *J Med Imaging Radiat Oncol*, vol. 65, no. 5, pp. 545–563, Aug. 2021, doi: 10.1111/1754-9485.13261.

[11] O. Ronneberger, P. Fischer, and T. Brox, "U-Net: Convolutional Networks for Biomedical Image Segmentation," May 2015.

[12] A. Sekuboyina *et al.*, "VERSE: A Vertebrae labelling and segmentation benchmark for multi-detector CT images," *Medical Image Analysis*, vol. 73. Elsevier B.V., Oct. 01, 2021. doi: 10.1016/j.media.2021.102166.

[13] M. T. Löffler *et al.*, "A vertebral segmentation dataset with fracture grading," *Radiol Artif Intell*, vol. 2, no. 4, pp. 1–6, 2020, doi: 10.1148/ryai.2020190138.

[14] H. Liebl *et al.*, "A computed tomography vertebral segmentation dataset with anatomical variations and multi-vendor scanner data," *Sci Data*, vol. 8, no. 1, Dec. 2021, doi: 10.1038/s41597-021-01060-0.

[15] C. Heidt, T. Angst, P. Büchler, C.-C. Hasler, and D. Studer, "Traditional T1-S1 Measurement of the Spinal Length on X-ray Images Does Not Correlate With the True Length of the Spine," *Int J Spine Surg*, vol. 16, no. 5, pp. 921–927, Oct. 2022, doi: 10.14444/8353.

[16] T. Vrtovec, B. Likar, and F. Pernuš, "Quantitative analysis of spinal curvature in 3D: application to CT images of normal spine," *Phys Med Biol*, vol. 53, no. 7, pp. 1895–1908, Apr. 2008, doi: 10.1088/0031-9155/53/7/006.

[17] C. G. T. Ledonio, B. E. Rosenstein, C. E. Johnston, W. E. Regelmann, D. J. Nuckley, and D. W. Polly, "Pulmonary function tests correlated with thoracic volumes in adolescent idiopathic scoliosis," *Journal of Orthopaedic Research*, vol. 35, no. 1, pp. 175–182, Jan. 2017, doi: 10.1002/jor.23304.

[18] Y. P. Charles, A. Marcoul, M. Schaeffer, F. Canavese, and A. Diméglio, "Three-dimensional and volumetric thoracic growth in children with moderate idiopathic scoliosis compared with normal," *Journal of Pediatric Orthopaedics Part B*, vol. 26, no. 3, pp. 227–232, 2017, doi: 10.1097/BPB.0000000000000393.

[19] C. J. Adam, S. C. Cargill, and G. N. Askin, "Computed Tomographic-Based Volumetric Reconstruction of the Pulmonary System in Scoliosis," *Journal of Pediatric Orthopaedics*, vol. 27, no. 6, pp. 677–681, Sep. 2007, doi: 10.1097/BPO.0b013e318425ee.

[20] W. C. W. Chu, B. K. W. Ng, A. M. Li, T. Lam, W. W. M. Lam, and J. C. Y. Cheng, "Dynamic magnetic resonance imaging in assessing lung function in adolescent idiopathic scoliosis: a pilot study of comparison before and after posterior spinal fusion," *J Orthop Surg Res*, vol. 2, no. 1, p. 20, Dec. 2007, doi: 10.1186/1749-799X-2-20.

[21] Y. Zeng *et al.*, "The influence of kyphosis correction surgery on pulmonary function and thoracic volume," *Spine (Phila Pa 1976)*, vol. 39, no. 21, pp. 1777–1784, Oct. 2014, doi: 10.1097/BRS.0000000000000524.

[22] M. M. A. Janssen *et al.*, "Pre-existent vertebral rotation in the human spine is influenced by body position," *European Spine Journal*, vol. 19, no. 10, pp. 1728–1734, Oct. 2010, doi: 10.1007/s00586-010-1400-3.